Journal of Inflammation Research

Dovepress
Taylor & Francis Group

Open Access Full Text Article

ORIGINAL RESEARCH

Macrophage-Derived Exosomal BMPR2 Mediates Alveolar Epithelial Repair and Cellular Crosstalk in Acute Lung Injury

Xiang Yun[1–3], Fei Li[1], Zhen Chen[4], Jiahua Meng[1], Lin Zhang[2,3,5], Juxiang Yuan[1]

[1]School of Public Health, North China University of Science and Technology, Tangshan, 063000, People's Republic of China; [2]Clinical Medical Research Center for Women and Children Diseases, Shandong Provincial Maternal and Child Health Care Hospital Affiliated to Qingdao University, Jinan, 250001, People's Republic of China; [3]Key Laboratory of Occupational Exposure and Fertility Preservation for Women of Shandong Health Commission, Shandong Provincial Maternal and Child Health Care Hospital Affiliated to Qingdao University, Jinan, 250001, People's Republic of China; [4]School of Public Health, Shandong second Medical University, Weifang, 261053, People's Republic of China; [5]Henan Medical Key Laboratory for Research of Trauma and Orthopedics, the Third Affiliated Hospital of Xinxiang Medical University, Xinxiang, 453000, People's Republic of China

Correspondence: Juxiang Yuan, School of Public Health, North China University of Science and Technology, Tangshan, 063000, People's Republic of China, Email yuanjx@ncst.edu.cn; Lin Zhang, Clinical Medical Research Center for Women and Children Diseases, Shandong Provincial Maternal and Child Health Care Hospital Affiliated to Qingdao University, Jinan, 250001, People's Republic of China, Tel +86-531-68795920, Email zhanglin8901@sdu.edu.cn

Background: Acute lung injury (ALI)/Acute respiratory distress syndrome (ARDS) continues to be a predominant cause of morbidity and mortality among critically ill patients, with few therapeutic options available. Although macrophage-derived exosomes have been identified as significant mediators of intercellular communication in tissue repair, their specific molecular mechanisms in the context of ALI remain inadequately understood. This study aims to investigate the role of macrophage-derived exosomes containing bone morphogenetic protein receptor 2 (BMPR2) in promoting the repair of blast-induced acute lung injury.

Methods: We established an in vitro blast injury model utilizing MLE-12 alveolar epithelial cells and isolated exosomes from J774A.1 macrophages through ultracentrifugation. Coculture experiments were conducted to evaluate cellular repair mechanisms, while molecular docking simulations were employed to predict protein interactions. We utilized cellular thermal shift assay (CETSA) analysis, Western blotting, and immunofluorescence to characterize the effects of exosomes on epithelial cell function and signaling pathways.

Results: Macrophage-derived exosomes, with a diameter of 169.7 ± 61.6 nm, significantly enhanced the viability of alveolar epithelial cells, reduced apoptosis, and promoted proliferation following blast injury. Proteomic analysis identified BMPR2 as the predominant effector protein, with an LG score of 5.182. Molecular docking studies revealed stable binding interactions between BMPR2 and BMPR1B. Functionally, exosomes facilitated the transdifferentiation of alveolar type II (AT2) cells to type I (AT1) cells through the activation of the TGF-β signaling pathway via the BMPR1B-SMAD1-ID1 axis, thereby promoting epithelial repair and regeneration.

Conclusion: This study establishes that exosomal BMPR2 derived from macrophages serves as a previously unrecognized paracrine signaling mechanism facilitating cellular crosstalk during ALI repair. The BMPR2-mediated signaling pathway offers a promising therapeutic target for the treatment of ALI, paving the way for new avenues in clinical intervention.

Keywords: exosomal BMPR2, alveolar epithelial, cellular crosstalk, repair, acute lung injury

Introduction

Acute lung injury (ALI)/Acute respiratory distress syndrome (ARDS) is a life-threatening pulmonary disorder with persistently high mortality rates ranging from 35% to 46%, despite advancements in critical care therapeutics.[1] This condition represents a significant unmet medical need. Among the various subtypes of ARDS, blast-induced lung injury (BLI) poses the most severe clinical challenge. It is characterized by pressure wave-induced alveolar rupture, extensive pulmonary hemorrhage, and profound oxidative stress responses that initiate complex inflammatory cascades involving neutrophil infiltration, pro-inflammatory cytokine release, and activation of damage-associated molecular patterns.[2,3] The

Received: 21 July 2025
Accepted: 18 October 2025
Published: 25 October 2025

high clinical burden of BLI is evidenced by its variable incidence (1.4–40%) and mortality rates surpassing 50% in critical cases, with China reporting 2098 blast-related incidents from 2000 to 2017 alone.[4,5] Current therapeutic strategies are inadequately supportive, primarily relying on mechanical ventilation and fluid management, without effective molecular-targeted treatments. This therapeutic gap, combined with the devastating clinical outcomes and the increasing global exposure to blast injuries, creates an urgent imperative for the development of novel therapeutic approaches that target the fundamental cellular and molecular mechanisms underlying BLI pathogenesis.[6,7]

The effective resolution of lung injury fundamentally requires the restoration of alveolar epithelial integrity via sophisticated intercellular communication networks, wherein alveolar macrophages function as pivotal regulators that coordinately modulate both pro-inflammatory cascades and tissue regenerative pathways, thereby maintaining pulmonary immunometabolic homeostasis.[8] These functional plastic immune cells represent the main business of innate immunization in the lung and respond to harm through strategic secretion of regulators, especially the transformation of growth factor β (TGF-β). The TGF-β-mediated answer coordinates necessary repair mechanisms, including extracellular matrix remodeling, fibroblast proliferation and myofibroblast differentiation, to restore the integrity of the alveolar barrier. The reciprocal crosstalk between alveolar epithelial type II cells (AEC2s) and tissue-resident macrophages constitutes a fundamental mechanistic paradigm in pulmonary repair, wherein this cellular interplay orchestrates homeostatic maintenance and regenerative responses through dynamically regulated signaling networks.[9,10]

Recent discoveries regarding exosomes (30–150 nm) have revolutionized our understanding of macrophage-epithelial communication.[11,12] These lipid bilayer-enclosed nanoscale vesicles act as sophisticated mediators of intercellular signaling and tissue regeneration. Functioning as specialized biological delivery systems, exosomes transport a diverse array of molecular cargo, including nucleic acids, proteins, lipids, and metabolic intermediates between cells.[13,14] Through the action of membrane-bound ligands and adhesion molecules, exosomes facilitate precise cellular communication with significant therapeutic potential. They demonstrate capabilities to modulate inflammatory responses, regulate cell survival pathways, and promote tissue regeneration. Importantly, emerging evidence suggests that macrophage-derived exosomes play a crucial role in the dialogue between epithelial and immune cells by modulating the TGF-β signaling pathway. For instance, exosomal miR-146a has been shown to enhance therapeutic outcomes in sepsis models, indicating potential analogous mechanisms in lung injury repair.[15,16]

Within this exosome-mediated communication framework, BMPR2 has emerged as a critical molecular switch governing cellular crosstalk and tissue homeostasis.[17] As a central component of the BMP signaling pathway within the TGF-β superfamily, BMPR2 plays essential roles in cellular differentiation, proliferation, and tissue repair processes. Research has shown that BMP is a secreted growth factor that regulates stem cell differentiation. Studies have demonstrated that BMP functions as a secreted growth factor regulating stem cell differentiation. Upon binding to its cognate receptors, BMP initiates intracellular signal transduction primarily through the SMAD signaling pathway.[18] Another study found that BMP/SMAD signaling, which mediates AT2 to AT1 differentiation during alveolar regeneration, can regulate ATII proliferation and promote differentiation, and discovered a new transitional cell state characterized by activation of TGF β and other pathways.[19,20] Single-cell RNA sequencing analyses have established the TGF-β signaling pathway as a central molecular hub governing functional regulation and network-level signaling interactions in lung repair processes.[21] However, despite the recognized importance of macrophage-derived exosomes in tissue repair and BMPR signaling in cellular differentiation, the specific therapeutic potential of exosomal BMPR2 in mediating intercellular communication during blast-induced acute lung injury remains unexplored.

Based on the important established role of macrophages in pathophysiology process of ALI, we hypothesis that macrophage-derived exosomes facilitate targeted cell-cell communication to repair BLI by specific effects on alveolar epithelial cells, with exosomal BMPR2 serving as a crucial mediator in this therapeutic mechanism. To investigate this hypothesis, we employed a comprehensive approach that combined single-cell sequencing to identify relevant cell populations and key signaling pathways, alongside the isolation and characterization of exosomes derived from mouse monocyte-macrophage J774A.1 cells, and an evaluation of their therapeutic efficacy using in vitro models of blast lung injury. This study aims to delineate the mechanisms by which macrophage-derived exosomal BMPR2 mediates cellular crosstalk between immune cells and the injured alveolar epithelium. This research may offer novel therapeutic strategies

for BLI treatment and enhance our understanding of the cellular communication networks essential for lung repair and regeneration following explosive injury.

Methods and Materials

Alveolar Epithelial Cells and in vitro Shock Wave Model Establishment

This study belongs to the experimental nature of inanimate matter and does not involve any human or animal samples. Therefore, ethical approval has been exempted by the Institutional Ethics Committee of Shandong Maternal and Child Health Hospital. Based on their physiological relevance to explosion-induced lung injury, we employed an in vitro gas explosion model utilizing two cell lines: the alveolar type II epithelial cell line MLE-12 (STCC20008P-1, Servicebio, Wuhan, China) and the mouse mononuclear macrophage cell line J774A.1 (CL-3070, ProCell, Wuhan, China). Alveolar epithelial cells, particularly AEC2, maintain critical physical and biological barriers within the alveoli. Following alveolar epithelial damage, AEC2 cells demonstrate both self-renewal capacity and the ability to differentiate into type I cells, facilitating tissue repair processes. These characteristics make MLE-12 cells particularly suitable as the primary component of our in vitro model, as they effectively represent alveolar epithelial cells directly affected by gas explosions. To validate functional effects observed in damaged MLE-12 cells, we incorporated J774A.1 macrophages into our model. These cells were selected for their essential role in maintaining alveolar homeostasis and their remarkable plasticity in transitioning between pro- and anti-inflammatory states in response to microenvironmental changes, thereby facilitating both inflammation resolution and tissue repair.

The experimental protocol involved culturing both cell lines in their respective media supplemented with 10% FBS and 5% penicillin-streptomycin. MLE-12 cells were maintained at a concentration of 2.5×10^5 cells/mL in F12 medium and incubated at 37°C in a 5% CO_2 atmosphere. To simulate explosion conditions, cell suspensions were transferred to sterile 5 mL EP tubes and sealed. The tubes were then inverted and positioned on the warhead of a shock wave therapy device (HM08CJ, Haomeng Orthopedic Equipment Factory, Guangdong, China) using a coupling agent. The experimental parameters were standardized at 8 bar pressure and 10 Hz frequency, with cells subjected to 1000 shock waves combined with high-temperature exposure (100°C for 40seconds) to replicate conditions within the shock tube. Following shock wave exposure, cells were seeded in 96-well plates at various concentrations according to specific experimental requirements. Model validation was conducted using predetermined assessment criteria.

Isolation and Characterization of J774A.1 Macrophage-Derived Exosomes

To investigate the functional significance of macrophage-secreted exosomes in cellular repair processes, we established a standardized isolation protocol employing differential ultracentrifugation with J774A.1 murine macrophages. Initial cell culture conditions were optimized by allowing J774A.1 cells to reach >95% confluency, thereby maximizing exosome production. To minimize interference from bovine serum exosomes, cell cultures were systematically switched to serum-depleted medium and incubated for 12 hours before harvesting conditioned media for subsequent exosome purification.

The exosome purification procedure employed a multi-step centrifugation strategy to achieve progressive separation of extracellular vesicles from cellular debris. The initial clarification steps included sequential centrifugation at increasing centrifugal forces: 500 g (10 min) to remove intact cells, 2000 g (15 min) for cellular debris elimination, and 10,000 g (30 min) to pellet larger microvesicles. The clarified supernatant was subsequently filtered through a 0.22 μm pore-size membrane to exclude residual particulates. Final exosome enrichment was accomplished by ultracentrifugation at 120,000 g for 70 min, with the obtained pellet subjected to PBS washing and resuspension. Aliquots of purified exosomes were preserved in 1.5 mL microcentrifuge tubes at −80°C until further analysis. For quality control, the isolated vesicles underwent rigorous characterization using complementary techniques. Transmission electron microscopy provided ultrastructural visualization of exosome morphology, while nanoparticle tracking analysis coupled with dynamic light scattering enabled precise quantification of vesicle size distribution and population density. The colloidal stability of the macrophage-derived exosomes was evaluated using a Malvern potential detector to ensure sample integrity for downstream applications.

Cell Counting Kit-8 (CCK-8) Assay for Cell Viability

MLE-12 cells at 80–90% confluence were suspended and divided into control and blast groups. For the blast group, MLE-12 cells (2.5×10^4 cells/well) were seeded in 96-well plates and cultured for 6 or 24 hours after intervention (8 bar, 10 Hz, 100°C for 40s). Next, 100 μL/mL of CCK-8 working solution was added to each well, with three cell - free wells as blank controls. The control group was left untreated. The reaction system was incubated at 37°C with 5% CO_2 for 2 h, after which the plate was immediately wrapped in aluminum foil to terminate the reaction. The microplate reader was preheated for 30 min before detection. Cell viability was quantified by ΔOD value at 450 nm (reference wavelength 650 nm) after subtracting the blank value.

Cell Viability Assessment by Calcein AM/PI Dual Fluorescence

Adherent cells were enzymatically dissociated using 0.25% trypsin (1 mL) for 30 seconds. Digestion was immediately quenched with 2 mL serum-supplemented complete medium upon visible cell detachment. The resulting suspension was centrifuged (160 g, 5 min, RT) and resuspended in fresh complete medium (1 mL). Cellular concentration was quantified using an automated cell counter. MLE-12 cells were plated in 96-well plates at 2.5×10^5 cells/mL (100 μL/well) and maintained under standard culture conditions (37°C, 5% CO_2) for 6 h or 24 h. At each endpoint, cultures were incubated with Calcein AM/PI solution (10 μL/mL final concentration) protected from light for 30 min. Fluorescent images were acquired through multi-field scanning using the ImageXpress Micro Confocal system. All procedures were conducted under low-light conditions to prevent fluorochrome degradation.

Immunofluorescence Assay

Cellular specimens were initially fixed with 4% paraformaldehyde (10 min, RT) and subsequently washed thrice with PBS (5 min each). Membrane permeabilization was achieved through 0.3% Triton X-100 treatment (15 min, RT), followed by additional PBS washes. To minimize nonspecific antibody interactions, samples were blocked with 10% normal goat serum (60 min, RT). Primary antibodies were then applied and allowed to incubate overnight at 4°C in light-protected conditions. After thorough washing to remove unbound primary antibodies, fluorophore-conjugated secondary antibodies were introduced for 2 hours at room temperature in darkness. Nuclear counterstaining was performed using Hoechst 33342 (15 min, RT). To determine the optimal TGF-β1 concentration and treatment duration for promoting AT2 alveolar epithelial cell transdifferentiation into AT1 cells, we established experimental groups with graded TGF-β1 concentrations (0, 10, 20, and 40 ng/mL) and treated MLE-12 cells for 24 or 48 hours. Cellular differentiation was assessed by quantifying the fluorescence expression intensity of type I and type II alveolar epithelial cell-specific protein markers. Fluorescent signals were ultimately captured and analyzed using the ImageXpress Micro Confocal imaging system.

Immunohistochemistry Assay

Cells from different treatment groups were inoculated into a 24-well plate at a density of 9×10^5 cells per well and cultured for 48 hours. After washing with PBS, the cells were fixed with 4% paraformaldehyde at room temperature for 10 minutes. Following this, the cells were permeabilized with 0.3% Triton X-100 at room temperature for 15 minutes and then blocked with 10% goat serum at room temperature for 60 minutes. After washing with PBS for 15 minutes, the secondary antibody was applied at room temperature for 120 minutes, followed by three PBS washes. The cells were then stained with 100 μL of DAB for 10 minutes in the dark at room temperature. After thorough washing with ending water, the cells were counterstained with hematoxylin (100 μL, 3 minutes) for visualization. Finally, the slides were washed with ending water and differentiated with a differentiation solution for 10 seconds.

Western Blot Assay

Total proteins were extracted from cells by RIPA lysis buffer and the protein concentration was quantitated by BCA protein assay reagent. Denaturation was achieved by heating protein lysates (4:1 sample/loading buffer ratio) at 100°C for 10 min. Electrophoretic separation was performed on appropriately concentrated SDS-polyacrylamide gels, initiating at 80 V for stacking and completing at 120 V for resolution. Proteins were subsequently transferred to methanol-activated

PVDF membranes under constant current (230 mA, transfer duration adjusted according to target protein molecular weights). Following three 7-min TBST washes, membranes were blocked with 5% non-fat dry milk (60 min, RT). Immunodetection involved sequential incubations with primary antibodies (overnight, 4°C) and horseradish peroxidase-conjugated secondary antibodies (60 min, RT), each followed by TBST washes. Protein bands were visualized using enhanced chemiluminescence (ChemiDoc MP Imaging System) and quantified with ImageJ software.

Cell Migration Assay

MLE-12 cells at 80–90% confluence was processed into suspension and divided into control and blast groups according to model parameters. Cells were seeded at 3×10^5 cells per well in 6-well plates pre-marked with three horizontal reference lines. After 6-hour attachment, vertical scratches were created using 200 μL pipette tips. Following PBS washing to remove debris, cells were maintained in 1% FBS medium. Wound closure was monitored at 0, 12, 24, 36, and 48 hours using an IX73 optical microscope, with healing quantification performed via ImageJ software.

Cell Proliferation Assay

MLE-12 cells were plated in 96-well plates at a density of 2.5×10^4 cells/well and pre-cultured for 6 hours prior to treatment. Following incubation with 100 μL EdU-555 (C0075S, Beyotime, China) working solution (20 μM) at 37°C for 2 hours, cells were fixed with 50 μL of 4% paraformaldehyde for 10 minutes at room temperature. To enhance membrane permeability, cells were then treated with 50 μL of 0.3% Triton X-100 for 10 minutes. EdU-fluorophore conjugation was achieved through a 30-minute click reaction at room temperature, after which nuclei were counterstained with Hoechst 33342 (5 μg/mL) for 10 minutes. Confocal imaging and quantitative analysis were performed using the ImageXpress Micro Confocal High-Content Imaging System (Molecular Devices).

Fluorescent Labeling Method Was Used to Observe the Uptake of Exosomes

Exosomes derived from J774A.1 macrophages were fluorescently labeled with DiO (C6, Uelandy, China) by incubating at room temperature for 4 hours. The labeled exosomes (10 μL/well) were then co-cultured with alveolar epithelial type II cell line MLE-12 in a humidified incubator (37°C, 5% CO_2) for 2 hours. Subsequently, cells were stained with SiR-Actin (CY-SC001, Cytoskeleton, USA) to visualize the cytoskeleton, followed by nuclear counterstaining with Hoechst 33342. Imaging was performed using the ImageXpress Micro Confocal System (Molecular Devices).

Establishment of Co-Culture System of Alveolar Epithelial Cells and Macrophages

The MLE-12 and J774A.1 cells were expanded to approximately 95% confluence in DMEM medium supplemented with 10% FBS under standard culture conditions. Following quantification using an automated cell counter, cells were allocated into control and blast groups. Seeding densities were adjusted according to the surface area ratio (2:0.32) between 24-well transwell plates (Corning 3470; 2 cm^2 basal area) and 96-well plates (0.32 cm^2/well). After subjecting MLE-12 cells to predetermined extracorporeal shock wave and hyperthermia injury parameters, we established a transwell co-culture system with J774A.1 macrophages in the upper chamber and injured MLE-12 epithelial cells in the lower chamber. The co-cultures were maintained under standard conditions for 6 and 24 hours prior to functional assessments, including CCK-8 viability assays, EdU proliferation tests, and apoptosis detection, with subsequent quantitative analysis performed using ImageJ software.

Cellular Thermal Shift Assay

MLE-12 cells were divided into Blast and Blast+Exo groups following standardized parameter modeling and seeded in 6-well plates. The Blast+Exo group was co-incubated with macrophage-derived exosomes for 4 hours to ensure complete exosome uptake. Cells were washed with PBS containing 1 mM protease inhibitor, resuspended in PBS, and adjusted to a density of 2.5×10^7 cells/mL. The cell suspension was equally divided into five aliquots and transferred to pre-labeled 1.5 mL microcentrifuge tubes for thermal stability assay. Each aliquot underwent temperature treatment in a pre-equilibrated metal bath at designated gradients (37°C, 45°C, 48°C, 50°C, and 53°C) for 3 minutes, followed by immediate ice quenching to arrest protein denaturation. Cellular proteins were

then extracted using RIPA lysis buffer supplemented with protease inhibitors, with subsequent centrifugation at 20,000 g for 20 minutes at 4°C to obtain clarified supernatants. After quantifying protein concentration via BCA assay, samples were denatured with Laemmli buffer at 100°C for 10 minutes. Equal protein loads (10 μg/lane) were resolved by SDS-PAGE and transferred to PVDF membranes for immunoblotting with target-specific antibodies. Band intensity quantification across temperature points enabled generation of thermal stability profiles through four-parameter logistic curve fitting (GraphPad Prism 9.4), providing thermodynamic characterization of protein interactions.

Statistical Analysis

All experimental data were processed using GraphPad Prism 9.4 and ImageJ 1.54f (National Institutes of Health) for statistical analysis and visualization. Continuous variables were first assessed for normal distribution using the Shapiro–Wilk test, with normally distributed data presented as mean ± standard deviation (SD). For comparisons between two independent groups, Student's *t*-test was employed, whereas one-way analysis of variance (ANOVA) was applied for multi-group comparisons. Upon detecting statistically significant intergroup differences ($P<0.05$ by ANOVA), post hoc analysis was performed using the Student-Newman-Keuls (SNK) method for pairwise comparisons. Semi-quantitative analyses of immunofluorescence (IF), immunohistochemistry (IHC), and Western blot (WB) images were conducted using the ImageJ image analysis system. A two-tailed *P*-value <0.05 was considered statistically significant for all tests unless otherwise specified.

Result

Establishment and Evaluation of an in vitro Model for Blast-Induced Acute Lung Injury

To delineate cellular dynamics in BLI, we reanalyzed single-cell RNA sequencing data from injured pulmonary tissues alongside matched controls.[22] A quantitative assessment of proportional changes and absolute cellular abundance revealed that alveolar macrophages (AMs), AT1, and AT2 pneumocytes were the predominant affected cell populations following injury. Through an integrated analysis that combined STRING protein-protein interaction networks with GeneRatio indices, we identified the TGF-β signaling pathway as the central molecular hub governing both functional regulation and network-level signaling interactions.[21]

To investigate the specific effects of blast exposure on alveolar epithelial cells, we established an in vitro model utilizing MLE-12 alveolar epithelial cells. Following our previous experimental protocols, cells were subjected to standardized blast conditions (8 bar, 10 Hz, 1000 cycles)[23] in conjunction with high-temperature treatment (Figure 1A). Assessment of cell viability through the CCK-8 assay revealed that MLE-12 cells exposed to the combined shock wave and high-temperature treatment for 40 seconds exhibited approximately (50 ± 5)% reduction in cell viability at 6 hours post-exposure compared to the control (0 s). Notably, MLE-12 cells demonstrated a gradual recovery in viability by 24 hours post-exposure (Figure 1B and C). These findings were further validated using Calcein-AM/PI dual staining, which confirmed the decreased viability of MLE-12 cells at 6 hours post-exposure compared to controls (Figure 1D and E). Additionally, the EdU assay indicated significant suppression of cell proliferation in treated MLE-12 cells at 6 hours, with both viability and proliferation exhibiting recovery patterns by 24 hours (Figure 1F and G). Based on these results, we established the combined shock wave exposure with 40-second high-temperature treatment (100°C) as the optimal parameters for subsequent experiments.

To evaluate the impact of combined shock wave and high-temperature exposure on MLE-12 cell motility, we conducted wound healing assays. The results demonstrated significantly reduced wound closure percentages in the exposed MLE-12 cells compared to the controls across all observed time points (Figure 1H and I). Collectively, these findings indicate that the combination of shock wave and high-temperature exposure significantly impairs the viability, proliferation, and motility of alveolar epithelial cells. Furthermore, the consistent cellular responses observed validate this approach as a reliable in vitro model for studying the mechanisms of BLI.

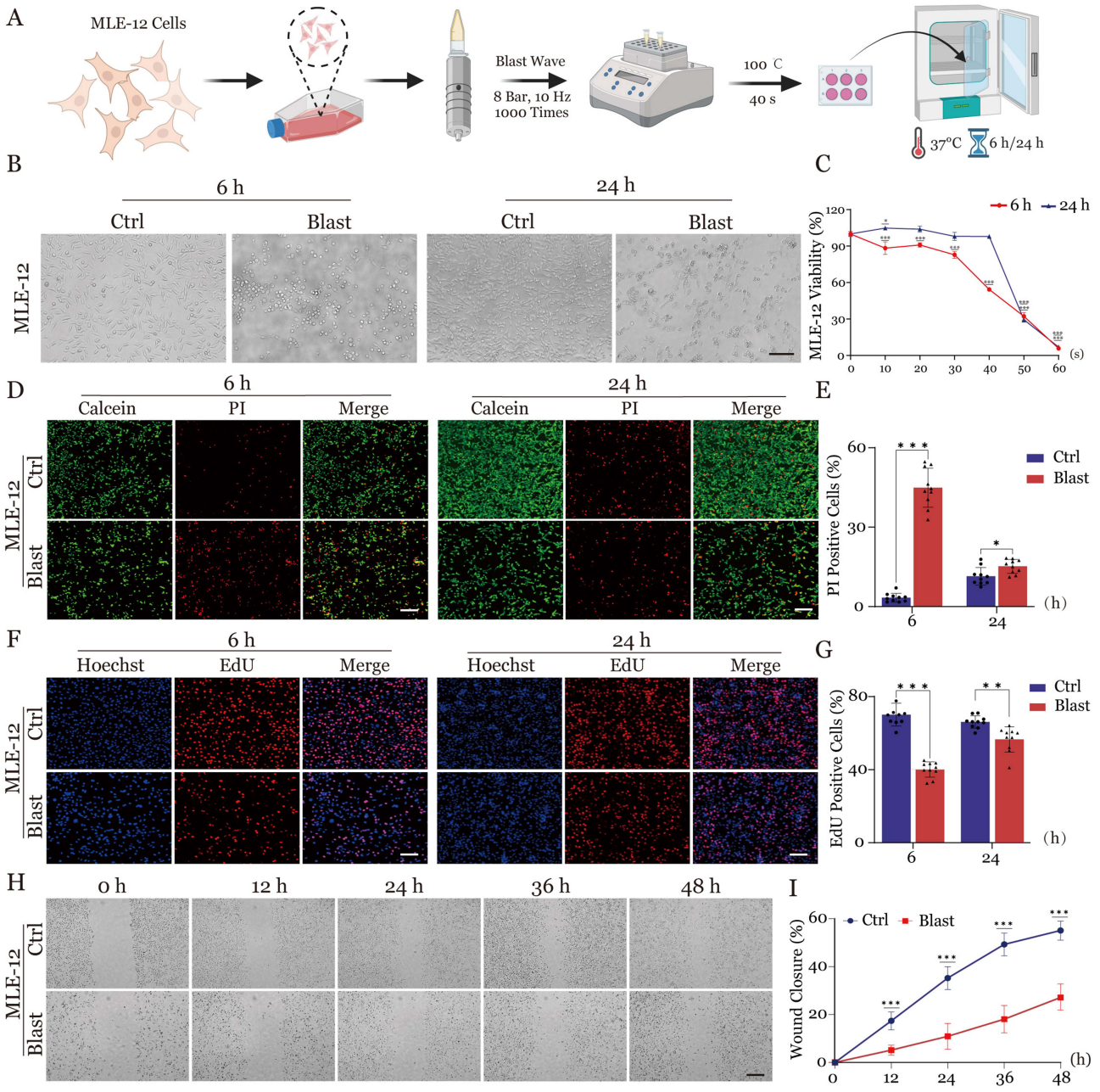

Figure 1 Establishment of an in vitro blast-induced lung injury model and its impact on cellular function. (**A**) Schematic illustration of the in vitro BLI model establishment. (**B**) Representative images showing morphological changes in MLE-12 cells at 6 and 24 hours post-blast exposure. Scale bar = 100 μm. (**C**) Cell viability assessment of MLE-12 cells, following blast exposure at different time points. Data are presented as mean ± SD. Statistical significance: **P* < 0.05, ****P* < 0.001 compared to corresponding 0 h groups. (**D**) Calcein-AM/PI double staining for cell viability analysis at 6 and 24 hours post-blast (green: viable cells; red: dead cells). Scale bar = 100 μm. (**E**) Quantification of PI-positive cells from the staining analysis. Statistical significance: **P* < 0.05, ****P* < 0.001 compared to corresponding control groups. (**F**) EdU proliferation assay showing cell proliferation status at 6 and 24 hours post-blast (blue: Hoechst-stained nuclei; red: EdU-positive cells). Scale bar = 100 μm. (**G**) Quantification of EdU-positive cells. Data are presented as mean ± SD. Statistical significance: ***P* < 0.01, ****P* < 0.001 compared to corresponding control groups. (**H**) Wound healing assay demonstrating cell migration capacity over 48 hours in control and blast-exposed MLE-12 cells. Scale bar = 100 μm. (**I**) Quantitative analysis of wound closure rates. Data are presented as mean ± SD. Statistical significance: ****P* < 0.001 compared to corresponding control groups.

Isolation, Characterization, and Alveolar Epithelial Uptake of Macrophage-Derived Exosomes

For exosome isolation and purification, the murine monocyte-macrophage cell line J774A.1 was selected and processed through differential ultracentrifugation (Figure 2A). Microscopic examination revealed that J774A.1 cells maintained consistent morphology and density under serum-free conditions compared to those in complete medium, displaying

https://doi.org/10.2147/JIR.S547454

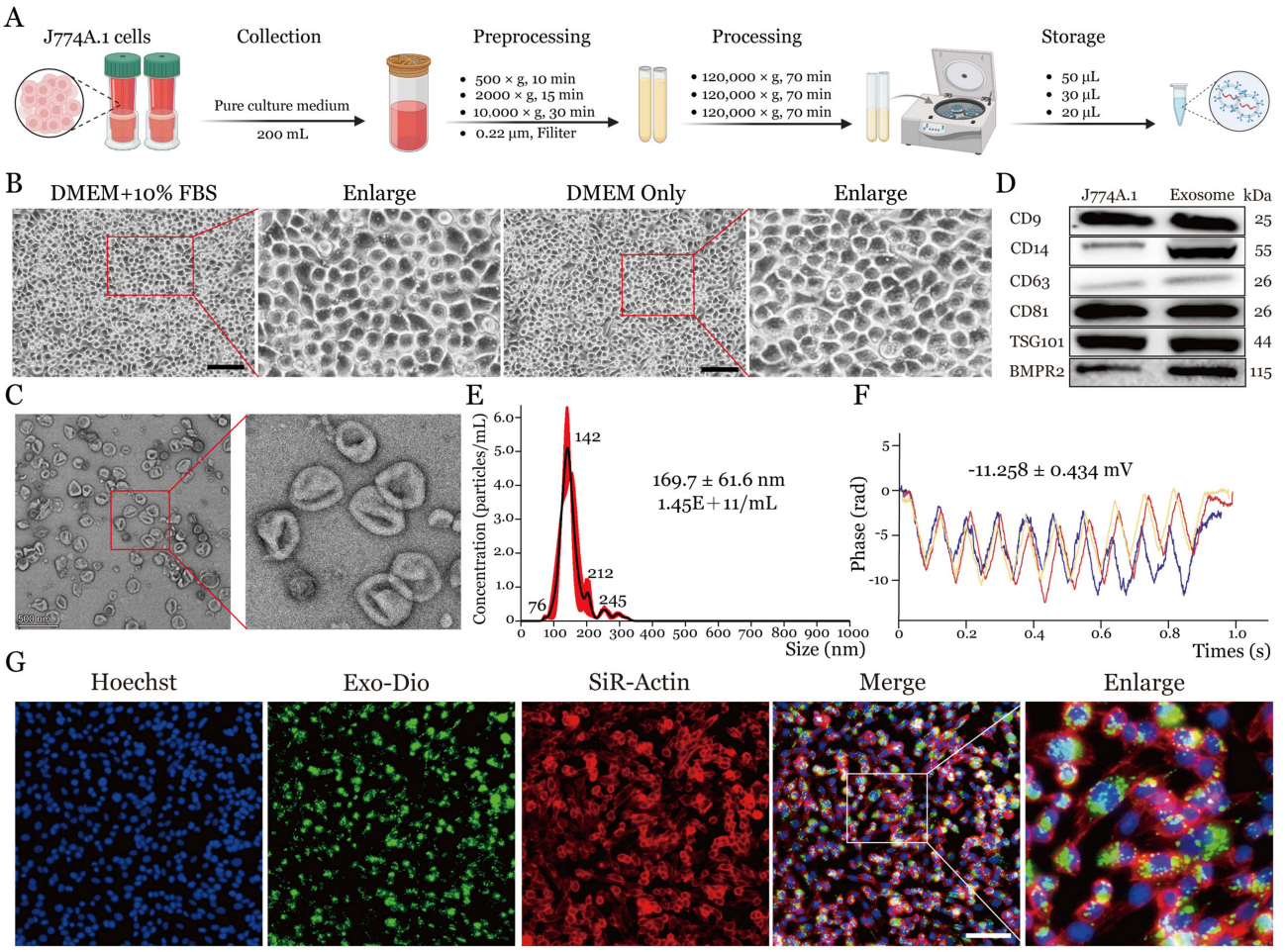

Figure 2 Isolation, characteristics, and uptake of extracellular vesicles from macrophages by lung epithelial cells. (**A**) Schematic workflow of exosome isolation from J774A.1 cells. (**B**) Phase-contrast microscopy images of J774A. 1 cells cultured in complete medium and serum-free conditions. Scale bar = 100 μm. (**C**) Transmission electron microscopy analysis of isolated exosomes showing characteristic morphology and size. Scale bar = 500 nm. (**D**) Western blot analysis of exosome marker proteins in both J774A.1 cells and isolated exosomes. (**E**) Nanoparticle tracking analysis showing size distribution of isolated exosomes. (**F**) Zeta potential measurement of isolated exosomes. (**G**) Fluorescence microscopy images demonstrating exosome uptake by MLE-12 cells (blue: Hoechst-stained nuclei; green: DiO-labeled exosomes; red: SiR-Actin). Scale bar = 200 μm.

a characteristic round morphology with clear margins and uniform distribution across the field of view. This observation indicates that short-term serum deprivation did not adversely affect cell viability (Figure 2B).

Transmission electron microscopy (TEM) analysis of the isolated vesicles revealed characteristic cup-shaped morphology with uniform round/oval profiles, observed both as discrete entities and aggregated clusters (Figure 2C). Subsequent Western blotting confirmed robust expression of canonical exosomal markers—including tetraspanins (CD9, CD14 CD63, CD81), endosomal sorting complex protein (TSG101), and BMPR2—validating vesicle identity (Figure 2D). Western blot analysis demonstrated a significant enrichment of BMPR2 protein in exosomes derived from J774A.1 macrophages, with the exosomal BMPR2 expression level showing a 1.826-fold increase compared to cellular levels (t=10.51, P<0.001). Quantitative characterization via nanoparticle tracking analysis (NTA) coupled with dynamic light scattering demonstrated a monodisperse population averaging 169.7 ± 61.6 nm in diameter at a concentration of 1.45×10^{11} particles/mL (Figure 2E). Furthermore, zeta potential measurements indicated stable colloidal dispersion with a mean surface charge of −11.258 ± 0.434 mV, consistent with exosome membrane electronegativity (Figure 2F).

To investigate exosome uptake by alveolar epithelial cells, we co-cultured DiO-labeled exosomes with MLE-12 cells, followed by SiR-Actin staining for cytoskeletal visualization and Hoechst nuclear counterstaining. Fluorescence microscopy revealed efficient membrane fusion and perinuclear accumulation of labeled exosomes, with minimal fluorescence

in cell-free regions, demonstrating the specific recognition and internalization of J774A.1-derived exosomes by MLE-12 cells (Figure 2G).

Cell Co-Culture Promotes Functional Recovery of Damaged Alveolar Epithelial Cell and Inhibits Cell Apoptosis

To evaluate the functional effects of macrophage-derived exosomes on MLE-12 cells, we established a co-culture system of MLE-12 and J774A.1 cells, assessing cell viability, apoptosis, and proliferation (Figure 3A–F). The results demonstrated that no statistically significant differences were observed in cell viability, proliferation rate, or apoptosis between the control group and the control+Exo group. In contrast, compared to the blast group, the blast+Exo group exhibited a significant increase in cell viability and proliferation, along with reduced apoptosis, with statistically marked differences between the two groups (Figure 3G–I). Collectively, these findings suggest that exosomes secreted by macrophages during co-culture could be effectively internalized by MLE-12 alveolar epithelial cells. The internalization of these extracellular vesicles markedly enhanced the survival and proliferation of injured alveolar epithelial cells while suppressing apoptotic activity.

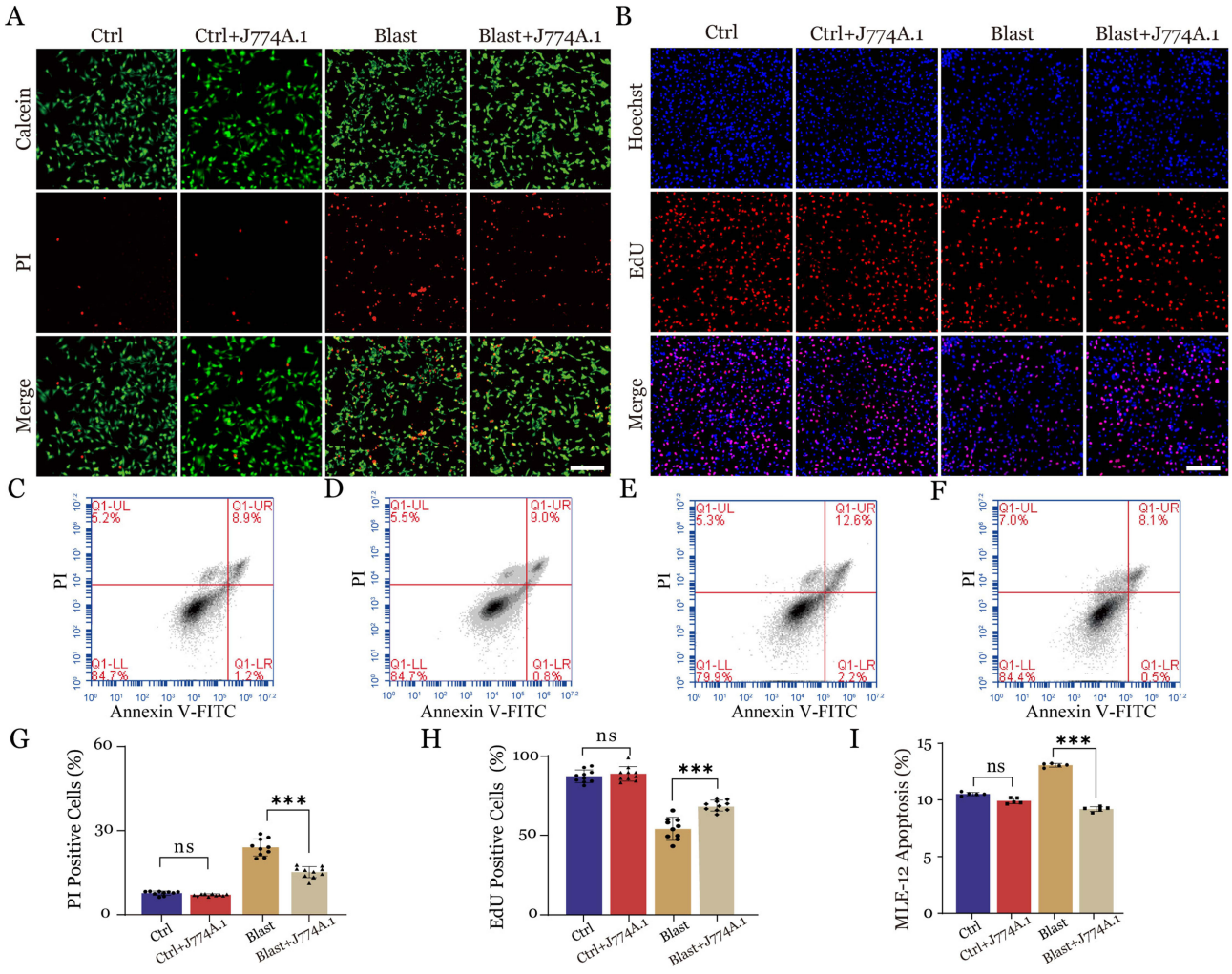

Figure 3 Analysis of the effect of cell co-culture system on the function of damaged lung epithelial MLE-12 cells. (**A**) Calcein-AM/PI double staining showing cell viability under exosome treatment conditions in different groups. Scale bar = 100 μm. (**B**) EdU proliferation assay results under exosome treatment conditions in different groups. Scale bar = 100 μm. (**C-F**) Annexin V-FITC/PI flow cytometry plots demonstrating apoptotic profiles across experimental conditions. (**G-I**) Quantitative comparisons of cell viability (**G**), proliferation rates (**H**) and apoptosis levels (**I**), respectively. Data are presented as mean ± SD. Statistical significance: ***$P < 0.001$, ns: not significant.

https://doi.org/10.2147/JIR.S547454

Macrophage-Derived Exosomes Promote Transdifferentiation of Type II to Type I Alveolar Epithelial Cells Following BLI

The transdifferentiation of alveolar AT2 to AT1 epithelial cells constitutes an essential repair mechanism in BLI. To elucidate the regulatory role of J774A.1 macrophage-derived exosomes in this process, we utilized our previously established in vitro blast injury model, which simulates combined shock wave and thermal exposure (Figure 4A). Epithelial injury dynamics were quantified through systematic analysis of cell type-specific markers: AGER (advanced

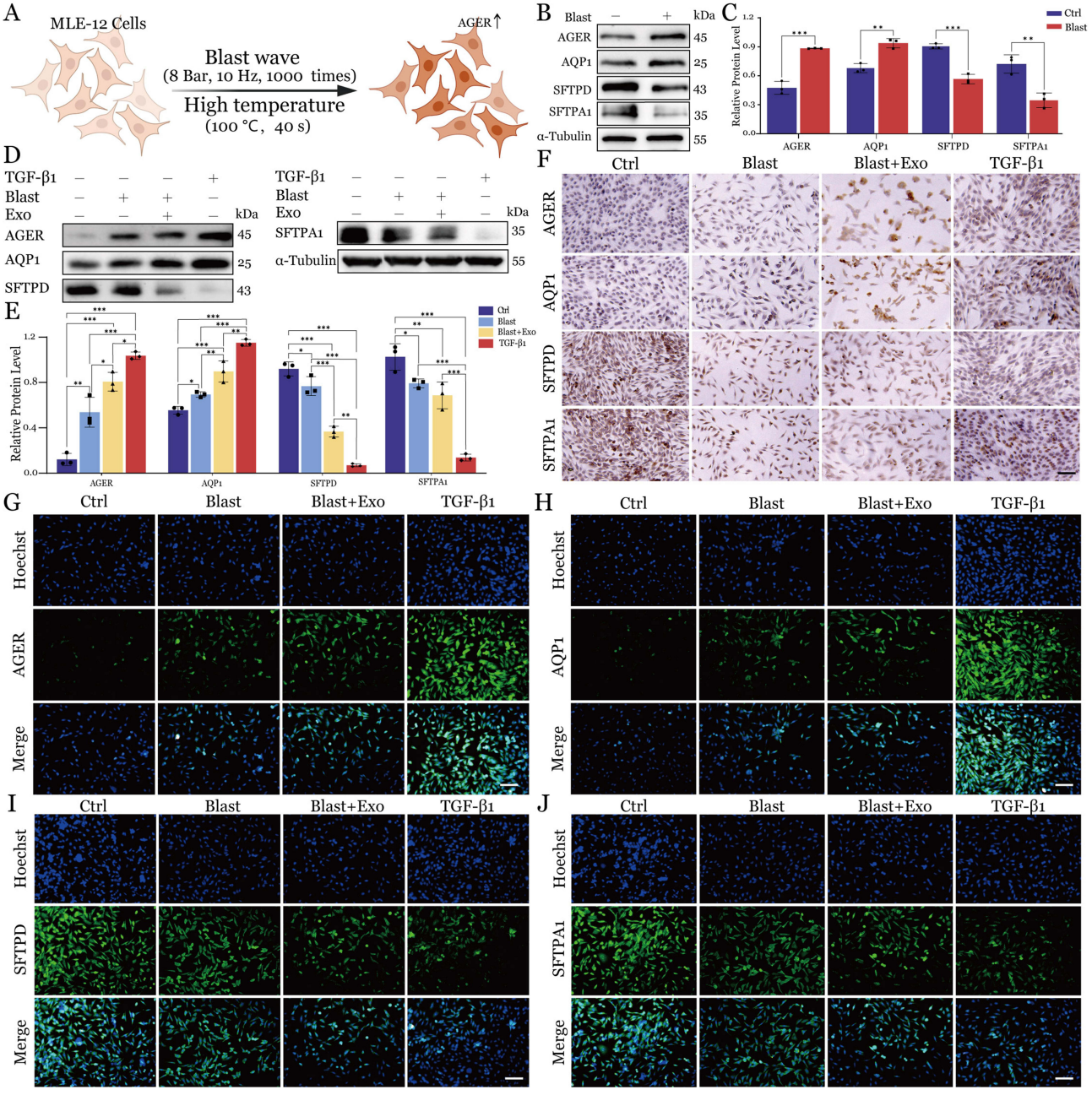

Figure 4 Macrophage-derived exosomes promote transdifferentiation of lung epithelial cells in the BLI model. (**A**) Schematic illustration of MLE-12 cells exposure to blast wave and high temperature conditions. (**B**) Western blot analysis of alveolar epithelial cell markers in control and blast-exposed cells. (**C**) Quantification of protein expression levels from Western blot analysis. Data are presented as mean ± SD. Statistical significance: $^{**}P < 0.01$, $^{***}P < 0.001$. (**D**) Western blot analysis of marker proteins in different experimental groups. (**E**) Quantitative analysis of protein expression levels across all treatment groups. Data are presented as mean ± SD. Statistical significance: $^{*}P < 0.05$, $^{**}P < 0.01$, $^{***}P < 0.001$. (**F**) Immunohistochemical staining showing expression patterns of marker proteins in different treatment groups. Scale bars = 200 μm. (**G-J**) Immunofluorescence analysis of alveolar epithelial cell markers across all experimental conditions (blue: Hoechst-stained nuclei; green: target proteins). Scale bars = 200 μm.

glycosylation end-product receptor) and AQP1 (aquaporin-1) for type I cells, and SFTPD (surfactant protein D) and SFTPA1 (surfactant protein A1) for type II cells. Western blot analysis demonstrated that MLE-12 cells subjected to blast conditions exhibited a marked increase in AT1 markers (AGER: 1.87-fold; AQP1: 1.38-fold) concurrent with significant downregulation of AT2 markers (SFTPD: 40% reduction; SFTPA1: 52.2% reduction) relative to untreated controls (Figure 4B and C). These data validate the efficacy of our in vitro system in recapitulating key pathophysiological features of blast-mediated alveolar epithelial damage, including phenotype transition and marker expression shifts.

To investigate the therapeutic potential of J774A.1 macrophage-derived exosomes in the repair of gas explosion-induced acute lung injury, we established four experimental groups: control (Ctrl), gas explosion (Blast), gas explosion with exosome treatment (Blast+Exo), and a TGF-β1 positive control group. Prior to the main experiments, we conducted preliminary dose-optimization studies. The optimal concentration for exosome intervention was determined through Calcein-AM/PI and EdU assays, which evaluated cell proliferation capacity (Figure S1A and B) and viability (Figure S1C and D) at four concentrations (0, 10, 100, and 200 μL/mL) after a 24-hour treatment. Based on comprehensive dose-response analyses, the concentration of 100 μL/mL was identified as exhibiting maximal biological efficacy while maintaining cellular viability, thereby being designated as the optimal working concentration for all subsequent experimental procedures. Moreover, our findings demonstrated that TGF-β1 treatment elicited concentration- and time-dependent modulation of alveolar epithelial markers, specifically upregulating type I cell marker AGER expression while suppressing type II cell marker SP-C expression. This inductive effect exhibited a progressive enhancement with both increasing TGF-β1 concentration and prolonged treatment duration (Figure S2A-D). These studies established 20 ng/mL for 24 hours as the optimal intervention parameters for the TGF-β1 positive control group (Figure S2E-H).

Semi-quantitative Western blot analysis demonstrated statistically significant differential expression profiles of target proteins across experimental groups, revealing distinct modulation patterns associated with specific treatment regimens. Relative to the control group, AGER and AQP1 protein expression levels progressively increased across the Blast, Blast +Exo, and TGF-β1 groups. In contrast, SFTPD and SFTPA1 protein levels exhibited a gradual decline across these groups (Figure 4D and E). These protein expression patterns were further proved through IF and IHC analyses. Immunohistochemical staining confirmed the progressive increase in AGER and AQP1 expression alongside the concurrent decrease in SFTPD and SFTPA1 levels across treatment groups relative to controls (Figures 4F and S3A). Similarly, immunofluorescence analysis demonstrated these reciprocal expression patterns (Figure 4G–J and Figure S3B-E), providing additional confirmation of the Western blot findings. These findings constitute the first experimental evidence that blast-induced acute lung injury initiates injured alveolar AT2 to AT1 cell transdifferentiation, a phenotypic conversion process markedly enhanced by exosomes derived from J774A.1 macrophages. Furthermore, these findings implicate the TGF-β signaling pathway as a key mediator in this cellular transformation process.

Structural and Functional Crosstalk Between Exosomal BMPR2 and Cellular BMPR1B Promotes Lung Epithelial Repair

To systematically investigate the cellular dynamics and receptor expression profiles in pulmonary injury models, with parallel identification of macrophage-derived exosomal therapeutic candidates, we implemented an integrated multi-omics approach combining single-cell RNA sequencing (scRNA-seq) with high-resolution tandem mass spectrometry (LC-MS/MS)-based proteomic analysis. Our preliminary investigations revealed a marked upregulation of BMPR1B expression in injured alveolar epithelial cells, demonstrating a 1.99-fold increase in transcript levels relative to control specimens.[21] This elevation was most pronounced in type II alveolar epithelial cells, which concurrently displayed alterations in characteristic cellular markers. Through integrative analysis employing the STRING protein-protein interaction database, we identified BMPR1B-centric signaling networks as a pivotal regulatory nexus in the injury response, establishing BMPR1B as a critical molecular node. To systematically characterize potential therapeutic vectors, we conducted high-resolution LC-MS/MS-based proteomic profiling of exosomes purified from J774A.1 macrophages, identifying 3603 distinct proteins. Gene ontology cellular component analysis classified 1247 proteins as membrane-associated, with BMPR2 ranking in the top 50%, confirming its position as the principal functional element of macrophage-derived exosomal cargo (Figure 5A).

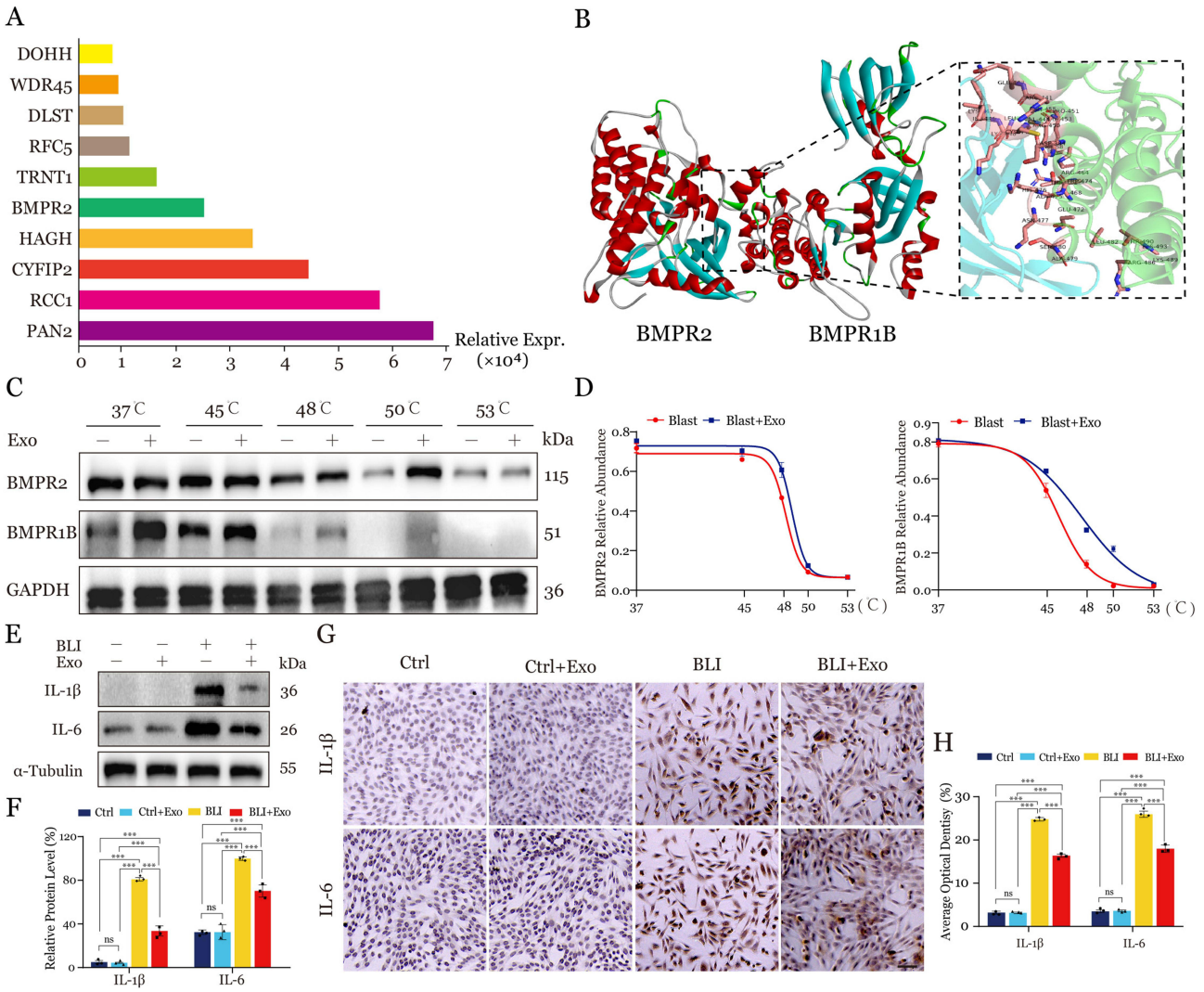

Figure 5 Integrated Single-Cell and Proteomic Analyses Identify BMPR1B Upregulation in Injured Alveolar Epithelium and BMPR2 Enrichment in Macrophage Exosomes. (**A**) Bar chart plot of representative genes packaged in exosomes. (**B**) Molecular docking of exosomal BMPR2 and alveolar BMPR1B. Enlarged view: Intermolecular interactions. (**C**) Western blot analysis of BMPR2 and BMPR1B protein expression under different temperature conditions in the presence or absence of Exosomes. (**D**) Relative abundance of BMPR2 and BMPR1B at different temperatures, assessed via CETSA. Data are represented as mean ± SD (n = 3). (**E**) Western spots showed protein expression of inflammation markers IL-1β and IL-6 in MLE-12 cells in various treatment groups. (**F**) Quantitative analysis of relative protein expression levels. Data are presented as mean ± SD. Statistical significance: ***$P < 0.001$; ns: no significant. (**G**) Immunohistochemical staining of MLE-12 cells reveals the expression patterns of IL-1β and IL-6 across different treatment groups. Nuclei are visualized in blue, while positive protein expression is indicated by brown-yellow staining. Scale bars = 200 nm. (**H**) Quantitative analysis of average optical density values of IL-1β and IL-6. Data are presented as mean ± SD. Statistical significance: ***$P < 0.001$; ns: no significant.

To elucidate the potential binding interface between exosomal BMPR2 and cellular BMPR1B, we performed in silico structural analyses through a two-tiered docking strategy. Initial molecular docking was conducted using AutoDock Vina with crystallographic structures of BMPR2 (PDB: 3G2F) and BMPR1B (PDB: 3MDY), generating 200 candidate conformations that were filtered by interaction energy and steric compatibility. For higher-resolution validation, we employed HDOCK—a hybrid algorithm integrating template-based and ab initio docking—to simulate BMPR2-BMPR1B interactions (Figure 5B). The top 10 HDOCK models demonstrated exceptional binding affinity (Docking Score: −230 ± 9.207; Confidence Score: 0.833 ± 0.024), with ligand RMSD values (94.96 ± 15.19 Å) indicating stable complex formation. Chemical cross-linking coupled with mass spectrometry identified multiple interprotein linkages at predicted interaction sites, corroborating the computational models. Structural metrics further confirmed the specificity of this interaction, with exosomal BMPR2 (LG score=5.182) and cellular BMPR1B (LG score=5.245) exhibiting complementary binding geometries. These data collectively provide atomistic evidence for BMPR2-BMPR1B recognition, suggesting its therapeutic relevance in acute lung injury pathogenesis.

To systematically characterize protein-ligand binding dynamics and quantitatively evaluate protein-protein interaction affinities, we implemented Cell Thermal Shift Assay (CETSA) for real-time monitoring of protein complex thermostability across a defined temperature gradient. By comparing the experimental data between the Blast group and the Blast+Exo group, we observed notable differences in their thermal stability fitting curve. In the Blast group, as the temperature increased from 37°C to 53°C, the expression of the BMPR2 protein exhibited a gradual decline. Notably, a significant reduction in BMPR2 signal intensity was observed when the temperature ranged from 45°C to 53°C (Figure 5C), indicating substantial pronounced denaturation and/or degradation occurring across the specified thermal regime. The distinct thermal profiles of BMP receptors reveal critical structural differences: BMPR2 displays marked thermolability, rendering its functional integrity vulnerable to environmental temperature variations or pathological stressors. In contrast, BMPR1B maintains conformational stability across physiological to febrile temperatures (37°C – 45°C), undergoing abrupt unfolding only upon exceeding 45°C (Figure 5D). Notably, Blast+Exo treatment conferred enhanced thermotolerance to both receptors, with the BMPR2-BMPR1B heterocomplex exhibiting synergistic stabilization—demonstrated rightward shift in thermal denaturation midpoints. This cooperative stabilization implies that heterodimerization may shield vulnerable domains through allosteric interactions or interfacial residue protection, potentially explaining its compensatory role in temperature-sensitive signaling pathways. To further validate the therapeutic potential of exosomal BMPR2 in alleviating inflammatory responses in lung epithelial MLE-12 cells, protein-level analyses were performed. Western blot analysis revealed a marked suppression of pro-inflammatory mediators IL-1β and IL-6 in the therapeutic cohort compared with BLI controls (Figure 5E and F). These observations were corroborated by cellular immunohistochemical staining, which consistently revealed reduced expression levels of both inflammatory markers (Figure 5G and H).

Macrophage-Derived Exosomes Mediate Lung Injury Repair Through TGF-β Signaling

Integrative analysis of single-cell RNA sequencing data, corroborated by established mechanistic studies, revealed the TGF-β signaling pathway as the pivotal regulator orchestrating AT2-to-AT1 transdifferentiation during BLI repair.[21–23] Specifically, BMP ligands within the TGF-β superfamily initiate a canonical signaling cascade through high-affinity binding to BMPRI/BMPRII heteromeric receptor complexes, triggering sequential phosphorylation and nuclear translocation of SMAD1/5/8 effectors to modulate transcriptional reprogramming. This cascade subsequently triggers the upregulation of ID1 expression, promoting the transdifferentiation of AT2 to AT1 and activating endogenous tissue repair mechanisms (Figure 6A). Therefore, investigating whether macrophage-derived exosomes facilitate pulmonary tissue repair through the TGF-β signaling pathway is crucial for elucidating the mechanisms underlying BLI repair.

Western blot analyses consistently demonstrated a pronounced suppression of NOGGIN expression in blast-exposed groups, contrasting with a concomitant elevation of BMPR1B and ID1 protein levels (Figure 6B and C). These observations collectively establish that exosomes derived from J774A.1 macrophages potentiate AT2-to-AT1 transdifferentiation in pulmonary tissues subjected to blast trauma, primarily through TGF-β pathway activation.

Discussion

This study elucidates the therapeutic role of macrophage-derived exosomes in BLI, revealing three key findings. First, we established an in vitro BLI model recapitulating hallmark pathological features, including progressive inflammation, alveolar epithelial damage, and dysregulated cell marker expression. Second, single-cell RNA sequencing analysis identified the TGF-β signaling pathway as the central orchestrator of reparative processes, with macrophage-derived exosomes specifically accelerating alveolar AT2-to-AT1 cell transdifferentiation—a critical repair mechanism. Third, mechanistic studies demonstrated that exosomal BMPR2 activates the BMPR1B-SMAD1-ID1 axis within the TGF-β pathway, providing a molecular basis for the observed epithelial repair. These findings collectively position macrophage-derived exosomes as novel paracrine mediators of alveolar regeneration in BLI.

Consistent with single-cell RNA sequencing data, alveolar macrophages and lung epithelial cells exhibited the most significant transcriptional alterations following injury. These findings are in agreement with previous observations by Xu Vanpala et al in chemically induced lung injury models.[24] However, our findings regarding epithelial cell population dynamics diverge from those reported by Hong et al, who documented a reduced proportion of alveolar epithelial cells in

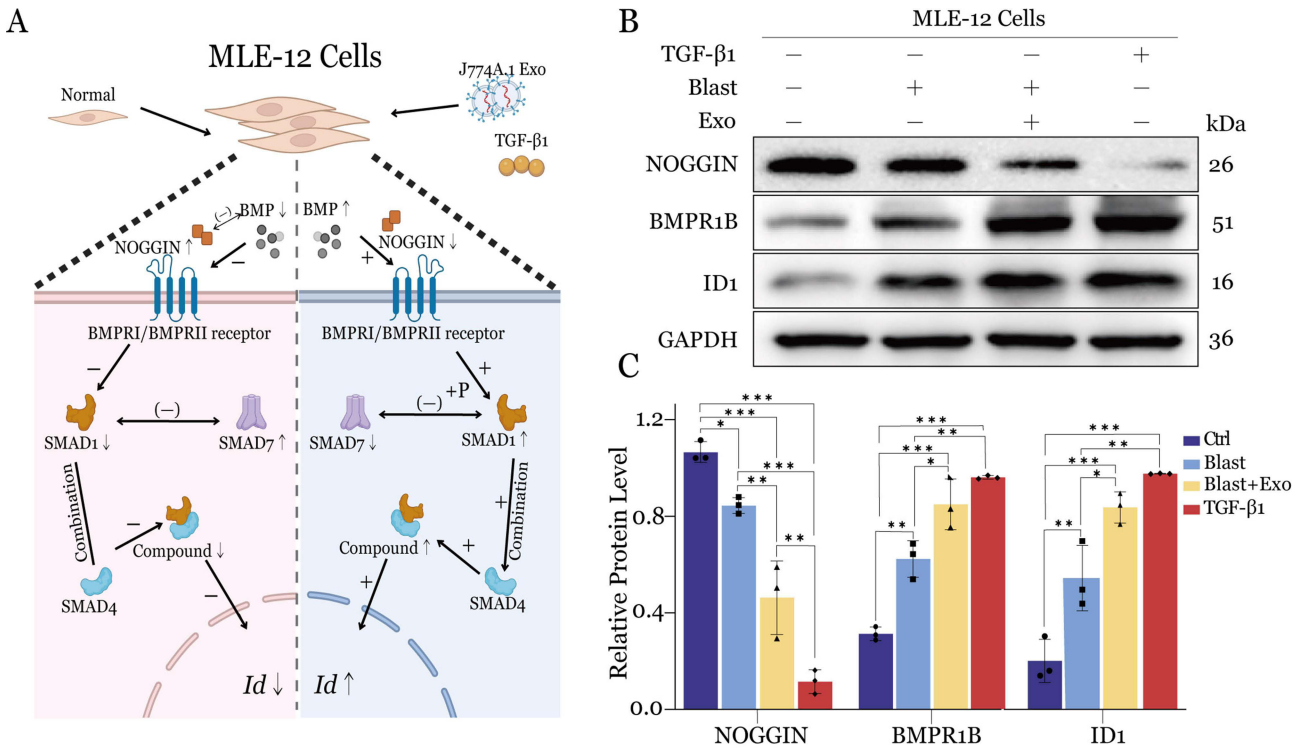

Figure 6 Role of TGF-β signaling pathway in macrophage exosome-mediated transdifferentiation of type II alveolar epithelial cells during BLI repair. (**A**) Schematic diagram illustrating the proposed mechanism of TGF-β signaling pathway regulation in MLE-12 cells by J774A.1-derived exosomes and TGF-β1. "+" indicates promotion of expression or activity; "-" indicates inhibition of expression or activity; "↑" represents an increase in protein expression; "↓" represents a decrease in protein expression. (**B**) Western blot analysis of key TGF-β pathway components in MLE-12 cells under different treatment conditions. (**C**) Quantitative analysis of protein expression levels from Western blot results in MLE-12 cells. Data are presented as mean ± SD. Statistical significance: $^{*}P < 0.05$, $^{**}P < 0.01$, $^{***}P < 0.001$.

radiation-induced lung injury.[25] This discrepancy likely reflects the unique pathophysiology associated with blast injury. Notably, our discovery of enhanced macrophage-epithelial cell communication networks extends beyond existing studies, such as those by Ye et al, who primarily focused on individual cell type responses.[26]

The characterization of macrophage-derived exosomes revealed distinct properties compared to previous studies. The observed size distribution (169.7 ± 61.6 nm) is larger than that reported by Chen et al for exosomes derived from M2 microglial cells (50–120 nm), yet it is consistent with findings from our previous study on activated macrophages.[14,27] The mechanism of exosome-mediated repair via TGF-β signaling constitutes a novel finding in the context of BLI treatment. While earlier studies by Liang et al demonstrated exosome-mediated repair in various lung injury models through anti-inflammatory mechanisms,[28] our identification of the BMPR1B-SMAD1-ID1 axis as a pivotal mediator of epithelial cell transdifferentiation offers new mechanistic insights. While this study validated the fundamental characteristics of extracellular vesicles using multiple technical methods to verify, two technical constraints should be noted. First, the preliminary scale of experimentation precluded assessment of negative controls including endoplasmic reticulum (calnexin) and Golgi apparatus (GM130) markers. Second, current methodologies cannot fully resolve extracellular vesicle subpopulations. Nevertheless, our optimized density gradient purification protocol demonstrated effective removal of major contaminants such as apoptotic bodies, thereby ensuring sufficient purity for functional validation.

This study acknowledges several limitations. In vitro experiments inherently fail to fully replicate the complex in vivo microenvironment and systemic regulatory networks. Specifically, the in vitro models lack critical influences present in lung tissue, such as multicellular crosstalk and the immune microenvironment. This absence may lead to an underestimation or overestimation of the actual regulatory effects of exosomes. While molecular docking and CETSA provide structural and thermodynamic evidence of BMPR2-BMPR1B interaction, the simplified in vitro co-culture system fails to recapitulate the complex systemic injury cascade triggered by concurrent blast wave and hyperthermia exposure. Furthermore, key aspects of exosome pharmacology remain unaddressed, including their in vivo metabolic kinetics and potential toxicity, which have not

been systematically assessed. These limitations underscore the necessity for future in vivo studies to validate the physiological relevance of the in vitro findings and to address gaps in the understanding of exosome toxicology. To address the current research limitations, future investigations should be comprehensively explored through the following key aspects. Future investigations should employ conditional knockout models or specific inhibitors in animal studies to establish causal relationships. Additionally, deeper mechanistic exploration of the BMPR2-BMPR1B-SMAD1-ID1 signaling cascade will be essential to fully understand the therapeutic potential of exosomal BMPR2 delivery. Although the TGF-β signaling pathway has been confirmed as pivotal, emerging proteomics data suggest that additional signaling mechanisms may cooperatively contribute to tissue repair processes, necessitating systematic mechanistic dissection.[29,30]

The enduring effects of exosome therapy on pulmonary function improvement and fibrotic complications remain elusive, particularly regarding delayed-onset complications. This situation warrants further investigation using refined animal models of lung injury. Building upon Ferguson et al's groundbreaking research on vesicular cargo composition, in-depth profiling of exosomal molecular payloads could unveil novel therapeutic targets.[31] Furthermore, exploring combinatory efficacy with conventional therapies, as demonstrated by Al-Hawary et al, is essential.[32] Leveraging recent advances in nanoparticle delivery technology to develop exosome delivery systems with enhanced tissue tropism and prolonged retention could holistically improve therapeutic outcomes.[33]

Conclusions

This study demonstrates that macrophage-derived exosomal BMPR2 plays a pivotal role in promoting alveolar epithelial repair following BLI. Through systematic in vitro modeling, we confirmed that exosomal BMPR2 enhances alveolar epithelial cell viability, reduces apoptosis, and facilitates AT2-to-AT1 transdifferentiation via the BMPR1B-SMAD1-ID1 axis within the TGF-β signaling pathway. These findings elucidate a novel paracrine mechanism by which macrophage exosomes mediate cellular crosstalk during ALI repair, offering a promising therapeutic target. While our in vitro blast injury model provides controlled experimental conditions and mechanistic insights, we explicitly acknowledge that these findings require validation in animal models to assess their physiological relevance. The therapeutic potential of BMPR2-containing exosomes should be considered preliminary until confirmed through in vivo studies.

Acknowledgment

The authors gratefully acknowledge Dr. Fucheng Zhu at the Medical Science and Technology Innovation Center of Shandong First Medical University & Shandong Academy of Medical Sciences for providing instrumental facilities and technical guidance.

Author Contributions

All authors made a significant contribution to the work reported, whether that is in the conception, study design, execution, acquisition of data, analysis and interpretation, or in all these areas; took part in drafting, revising or critically reviewing the article; gave final approval of the version to be published; have agreed on the journal to which the article has been submitted; and agree to be accountable for all aspects of the work.

Funding

This work was financially supported by the Taishan Scholar Program of Shandong Province (No. tsqn202211359). The funders had no role in study design, data collection, interpretation, or the decision to submit the work for publication.

Disclosure

The authors declare that there is no conflict of interest regarding the publication of this paper.

References

1. Mowery NT, Terzian WTH, Nelson AC. Acute lung injury. *Curr Probl Surg*. 2020;57(5):100777. doi:10.1016/j.cpsurg.2020.100777
2. Scott TE, Kirkman E, Haque M, Gibb IE, Mahoney P, Hardman JG. Primary blast lung injury - a review. *Br J Anaesth*. 2017;118(3):311–316. doi:10.1093/bja/aew385

3. Hamacher J, Hadizamani Y, Huwer H, et al. Characteristics of inflammatory response and repair after experimental blast lung injury in rats. *PLoS One*. 2023;18(3):e0281446. doi:10.1371/journal.pone.0281446
4. Broderick JC, Mancha F, Long BJ, Maddry JK, Chung KK, Schauer SG. Combat trauma-related acute respiratory distress syndrome: a scoping review. *Crit Care Explor*. 2022;4(9):e0759. doi:10.1097/cce.0000000000000759
5. Wang X, Du J, Zhuang Z, Wang ZG, Jiang JX, Yang C. Incidence, casualties and risk characteristics of civilian explosion blast injury in China: 2000-2017 data from the state Administration of Work Safety. *Mil Med Res*. 2020;7(1):29. doi:10.1186/s40779-020-00257-5
6. Butt Y, Kurdowska A, Allen TC. Acute lung injury: a clinical and molecular review. *Arch Pathol Lab Med*. 2016;140(4):345–350. doi:10.5858/arpa.2015-0519-RA
7. Qiao X, Yin J, Zheng Z, Li L, Feng X. Endothelial cell dynamics in sepsis-induced acute lung injury and acute respiratory distress syndrome: pathogenesis and therapeutic implications. *Cell Commun Signal*. 2024;22(1):241. doi:10.1186/s12964-024-01620-y
8. Yang G, Yang Y, Liu Y, Liu X. Regulation of alveolar macrophage death in pulmonary fibrosis: a review. *Apoptosis*. 2023;28(11–12):1505–1519. doi:10.1007/s10495-023-01888-4
9. Xue Y, Wang M, Han H. Interaction between alveolar macrophages and epithelial cells during mycoplasma pneumoniae infection. *Front Cell Infect Microbiol*. 2023;13:1052020. doi:10.3389/fcimb.2023.1052020
10. Song L, Li K, Chen H, Xie L. Cell cross-talk in alveolar microenvironment: from lung injury to fibrosis. *Am J Respir Cell Mol Biol*. 2024;71(1):30–42. doi:10.1165/rcmb.2023-0426TR
11. Zhang L, Tian J, Li N, et al. Exosomal miRNA reprogramming in pyroptotic macrophage drives silica-induced fibroblast-to-myofibroblast transition and pulmonary fibrosis. *J Hazard Mater*. 2025;483:136629. doi:10.1016/j.jhazmat.2024.136629
12. Chen Z, Xiong M, Tian J, Song D, Duan S, Zhang L. Encapsulation and assessment of therapeutic cargo in engineered exosomes: a systematic review. *J Nanobiotechnol*. 2024;22(1):18. doi:10.1186/s12951-023-02259-6
13. Tian J, Han Z, Song D, et al. Engineered exosome for drug delivery: recent development and clinical applications. *Int J Nanomed*. 2023;18:7923–7940. doi:10.2147/ijn.S444582
14. Chen Z, Yun X, Tian J, et al. Engineering macrophage-derived exosome to deliver pirfenidone: a novel approach to combat silicotic pulmonary fibrosis. *Adv Healthc Mater*. 2025;14(4):e2403227. doi:10.1002/adhm.202403227
15. Gong T, Liu YT, Fan J. Exosomal mediators in sepsis and inflammatory organ injury: unraveling the role of exosomes in intercellular crosstalk and organ dysfunction. *Mil Med Res*. 2024;11(1):24. doi:10.1186/s40779-024-00527-6
16. Zhang YG, Song Y, Guo XL, et al. Exosomes derived from oxLDL-stimulated macrophages induce neutrophil extracellular traps to drive atherosclerosis. *Cell Cycle*. 2019;18(20):2674–2684. doi:10.1080/15384101.2019.1654797
17. Ye Q, Taleb SJ, Zhao J, Zhao Y. Emerging role of BMPs/BMPR2 signaling pathway in treatment for pulmonary fibrosis. *Biomed Pharmacother*. 2024;178:117178. doi:10.1016/j.biopha.2024.117178
18. Carreira AC, Zambuzzi WF, Rossi MC, Astorino Filho R, Sogayar MC, Granjeiro JM. Bone morphogenetic proteins: promising molecules for bone healing, bioengineering, and regenerative medicine. *Vitam Horm*. 2015;99:293–322. doi:10.1016/bs.vh.2015.06.002
19. Aspal M, Zemans RL. Mechanisms of ATII-to-ATI cell differentiation during lung regeneration. *Int J Mol Sci*. 2020;21(9). doi:10.3390/ijms21093188
20. Chung MI, Bujnis M, Barkauskas CE, Kobayashi Y, Hogan BLM. Niche-mediated BMP/SMAD signaling regulates lung alveolar stem cell proliferation and differentiation. *Development*. 2018;145(9). doi:10.1242/dev.163014
21. Yun X, Chen Z, Li F, Shen F, Zhang L, Yuan J. Exosomal BMPR2 macromolecule facilitates alveolar epithelial cell repair through functional complex formation with BMPR1B in acute lung injury. *Int J Nanomed*. 2025;20:7233–7249. doi:10.2147/ijn.S519393
22. Zhang L, Wang Y, Tian L, et al. Thrombospondin-1-mediated crosstalk between autophagy and oxidative stress orchestrates repair of blast lung injury. *Biochim Biophys Acta Mol Basis Dis*. 2024;1870(3):167026. doi:10.1016/j.bbadis.2024.167026
23. Ding C, Hong S, Zhang M, et al. Establishment and evaluation of an in vitro blast lung injury model using alveolar epithelial cells. *Front Public Health*. 2022;10:994670. doi:10.3389/fpubh.2022.994670
24. Xu-Vanpala S, Deerhake ME, Wheaton JD, et al. Functional heterogeneity of alveolar macrophage population based on expression of CXCL2. *Sci Immunol*. 2020;5(50). doi:10.1126/sciimmunol.aba7350
25. Hong JH, Jung SM, Tsao TC, et al. Bronchoalveolar lavage and interstitial cells have different roles in radiation-induced lung injury. *Int J Radiat Biol*. 2003;79(3):159–167. doi:10.1080/0955300031000076894
26. Ye C, Yang X, Zhu L, Chang G, Hu Y, Wang W. Macrophage-derived exosomal miR-2137 regulates pyroptosis in LPS-induced acute lung injury. *Int Immunopharmacol*. 2024;143(Pt 3):113549. doi:10.1016/j.intimp.2024.113549
27. Chen C, Bao Y, Xing L, et al. Exosomes derived from M2 microglial cells modulated by 1070-nm light improve cognition in an alzheimer's disease mouse model. *Adv Sci*. 2023;10(32):e2304025. doi:10.1002/advs.202304025
28. Liang L, Peng W, Qin A, et al. Intracellularly synthesized artificial exosome treats acute lung injury. *ACS Nano*. 2024;18(32):21009–21023. doi:10.1021/acsnano.4c01900
29. Jackson M, Chen S, Liu P, et al. Quantitative proteomic profiling in brain subregions of mice exposed to open-field low-intensity blast reveals position-dependent blast effects. *Shock Waves*. 2024;34(4):381–398. doi:10.1007/s00193-024-01169-2
30. Li L, Liu Z, Tian L, et al. Single-cell proteomics delineates murine systemic immune response to blast lung injury. *Commun Biol*. 2024;7(1):1429. doi:10.1038/s42003-024-07151-z
31. Ferguson SW, Nguyen J. Exosomes as therapeutics: the implications of molecular composition and exosomal heterogeneity. *J Control Release*. 2016;228:179–190. doi:10.1016/j.jconrel.2016.02.037
32. Al-Hawary SIS, Alhajlah S, Olegovich BD, et al. Effective extracellular vesicles in glioma: focusing on effective ncRNA exosomes and immunotherapy methods for treatment. *Cell Biochem Funct*. 2024;42(1):e3921. doi:10.1002/cbf.3921
33. Li L, Wang F, Zhu D, Hu S, Cheng K, Li Z. Engineering exosomes and exosome-like nanovesicles for improving tissue targeting and retention. *Fundam Res*. 2025;5(2):851–867. doi:10.1016/j.fmre.2024.03.025